18

Integrated Controller Design for Automotive Semi-Active Suspension Considering Vehicle Behavior with Steering Input

Masaki Takahashi, Takashi Kumamaru and Kazuo Yoshida
Keio University,
Japan

1. Introduction

Semi active suspension control systems have recently been utilized to improve ride comfort of vehicles and their effectiveness has also been demonstrated (Ohsaku et al., 2000). However, it is not easy to improve simultaneously both ride comfort and steering stability when steering. To achieve it, several control methods have been proposed (Hrovat, 1993)-(Yoshida et al., 2006). In addition, because both ride comfort and steering stability greatly depend on the sensitivity of the human body to vibration, vehicle design that takes this and visual sensitivity into consideration is expected to be introduced. Furthermore, it has been reported that the phase difference in motion by pitching and rolling has an influence on steering stability and passenger ride comfort (Sakai et al., 2006)-(Kawagoe et al., 1997).

To improve both ride comfort and steering stability, this study proposes a controller design method for semi-active suspension system taking into consideration the most sensitive frequency range of the human body and vehicle behavior when steering. A method that can improve both the ride comfort and the vehicle stability is proposed by separating the control range in terms of the frequency domain, where the frequency weighting in controlled variables is used. Furthermore, the controller is scheduled in the time domain to attain a positive pitch angle during slaloms. The dynamics of road disturbance is assumed and is accommodated into the controller to make control more effective. In order to verify the effectiveness of the proposed method, a full-vehicle model that has variable stiffness and a damping semi-active suspension system is constructed and the numerical simulations are carried out. From the simulation results, it is demonstrated that the proposed method can improve ride comfort in the frequency domain that humans feel uncomfortable, reduce vehicle motion, and synchronize the roll and pitch angles caused by steering.

2. Modeling

A full-vehicle model which has variable stiffness and a damping semi-active suspension system is shown in Fig.1. The equations of motion are as follows:

$$
\begin{aligned}
&M_b\ddot{z}_g(t)=\sum_{i=1}^{4}f_{si}(t)\\
&M_{ti}\ddot{z}_{ui}(t)=-f_{si}(t)-K_{ti}z_{ti}(t)\quad (i=1,\cdots,4)\\
&I_p\ddot{\theta}_p(t)=-L_f(f_{s1}(t)+f_{s2}(t))+L_r(f_{s3}(t)+f_{s4}(t))+M_bgH_p\theta_p(t)-M_bH_p\ddot{x}_g(t)\\
&I_r\ddot{\phi}_r(t)=\frac{T_f}{2}(f_{s1}(t)-f_{s2}(t))+\frac{T_r}{2}(f_{s3}(t)-f_{s4}(t))+M_bgH_r\phi_r(t)+M_bH_r\ddot{y}_g(t)\\
&I_y\ddot{\psi}_y(t)=L_f(\sum_{i=1}^{2}f_{xi}(t)\sin\delta_f(t)+\sum_{i=1}^{2}f_{yi}(t)\cos\delta_f(t))-L_r(f_{y3}(t)+f_{y4}(t))\\
&M\ddot{x}_g(t)=\sum_{i=1}^{2}f_{xi}(t)\cos\delta_f(t)-\sum_{i=1}^{2}f_{yi}(t)\sin\delta_f(t)+\sum_{i=3}^{4}f_{xi}(t)-M_bH_p\ddot{\theta}_p(t)\\
&M\ddot{y}_g(t)=\sum_{i=1}^{2}f_{xi}(t)\sin\delta_f(t)+\sum_{i=1}^{2}f_{yi}(t)\cos\delta_f(t)+\sum_{i=3}^{4}f_{yi}(t)+M_bH_r\ddot{\phi}_r(t)
\end{aligned}
\tag{1}
$$

where H_p and H_r show the distance from the pitch rotation axis to the ground and the distance from the body center of gravity to the roll center respectively. f_{si} is the force that acts on the suspension of each wheel and is shown the following equation including the variable stiffness k_{si} and the variable damping c_{si}. f_{ai} is an output of the semi-active suspension system.

$$
\begin{aligned}
&f_{si}(t)=-K_f(t)z_{si}(t)-C_f(t)\dot{z}_{si}(t)+f_{ai}(t)\quad (i=1,2)\\
&f_{si}(t)=-K_r(t)z_{si}(t)-C_r(t)\dot{z}_{si}(t)+f_{ai}(t)\quad (i=3,4)\\
&f_{ai}(t)=-k_{si}(t)z_{si}(t)-c_{si}(t)\dot{z}_{si}(t)\quad (i=1,\cdots,4)
\end{aligned}
\tag{2}
$$

where $z_{si}(t)$ is the suspension stroke.

$$
\begin{aligned}
&z_{s1}(t)=z_g(t)-L_f(t)\theta_p(t)+T_f/2\phi_r(t)-z_{u1}(t)\\
&z_{s2}(t)=z_g(t)-L_f(t)\theta_p(t)-T_f/2\phi_r(t)-z_{u2}(t)\\
&z_{s3}(t)=z_g(t)+L_r(t)\theta_p(t)+T_r/2\phi_r(t)-z_{u3}(t)\\
&z_{s4}(t)=z_g(t)+L_r(t)\theta_p(t)-T_r/2\phi_r(t)-z_{u4}(t)
\end{aligned}
\tag{3}
$$

f_{xi} and f_{yi} show the longitudinal and lateral forces that act on the tire respectively and are derived from a nonlinear tire model of magic formula (Bakker et al., 1987), (Bakker et al., 1989). From the motion of equation in Eq. (1), the following bilinear system of 7 degree of freedom model for controller design is derived.

$$
\dot{\mathbf{x}}(t)=\mathbf{A}\mathbf{x}(t)+\mathbf{B}\mathbf{X}^*(t)\mathbf{u}(t)+\mathbf{E}_r\mathbf{w}(t)+\mathbf{E}_s\mathbf{f}_d(t)
\tag{4}
$$

where

$$
\begin{aligned}
&\mathbf{x}(t)=[z_g\ \theta_p\ \phi_r\ z_{u1}\ z_{u2}\ z_{u3}\ z_{u4}\ \dot{z}_g\ \dot{\theta}_p\ \dot{\phi}_r\ \dot{z}_{u1}\ \dot{z}_{u2}\ \dot{z}_{u3}\ \dot{z}_{u4}]^T\\
&\mathbf{X}^*(t)=diag(z_{s1}\ z_{s2}\ z_{s3}\ z_{s4}\ \dot{z}_{s1}\ \dot{z}_{s2}\ \dot{z}_{s3}\ \dot{z}_{s4})\\
&\mathbf{u}(t)=[k_{s1}\ \ k_{s2}\ \ k_{s3}\ \ k_{s4}\ \ c_{s1}\ \ c_{s2}\ \ c_{s3}\ \ c_{s4}]^T\\
&\mathbf{w}(t)=[w_1\ \ w_2\ \ w_3\ \ w_4]^T\\
&\mathbf{f}_d(t)=[f_{dp}\ \ f_{dr}]^T
\end{aligned}
$$

symbol	parameter	value
M	total mass	1598 kg
M_b	mass of body	1424 kg
M_{t1}, M_{t2}	mass of front tire	45 kg
M_{t3}, M_{t4}	mass of rear tire	42 kg
I_p	pitch moment of inertia	3500 kgm^2
I_r	roll moment of inertia	1019 kgm^2
I_y	yaw moment of inertia	3270 kgm^2
K_{t1}, K_{t2}	stiffness coefficient of front tire	190000 N/m
K_{t3}, K_{t4}	stiffness coefficient of rear tire	190000 N/m
K_f	stiffness coefficient (front, passive)	27000 N/m
K_r	stiffness coefficient (rear, passive)	28000 N/m
C_{t1}, C_{t2}	damping coefficient of front tire	0 Ns/m
C_{t3}, C_{t4}	damping coefficient of rear tire	0 Ns/m
C_f	damping coefficient (front, passive)	1500 Ns/m
C_r	damping coefficient (rear , passive)	1750 Ns/m
L_f	length from C.G. to axle (front)	1.22 m
L_r	length from C.G. to axle (rear)	1.46 m
T_f, T_r	length of track	1.52 m
H_p	pitch height	0.715 m
H_r	roll height	0.620 m
K_{fmin}	minimum value of variable stiffness coefficient (front)	11000 N/m
K_{fmax}	maximum value of variable stiffness coefficient (front)	100000 N/m
K_{rmin}	maximum value of variable stiffness coefficient (rear)	11000 N/m
K_{rmax}	maximum value of variable stiffness coefficient (rear)	102000 N/m
C_{fmin}	maximum value of variable damping coefficient (front)	100 Ns/m
C_{fmax}	maximum value of variable damping coefficient (front)	8000 Ns/m
C_{rmin}	maximum value of variable damping coefficient (rear)	450 Ns/m
C_{rmax}	maximum value of variable damping coefficient (rear)	8250 Ns/m

Table 1. Model Specification

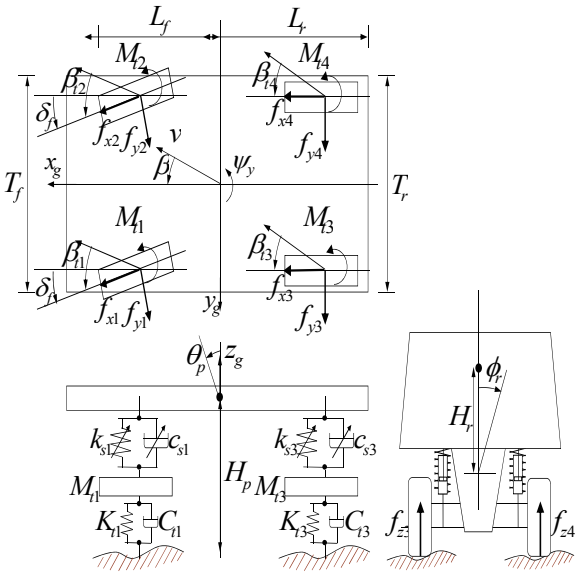

Fig. 1. Full Vehicle Model

In Eq. (4), the second term is the force which semi active suspension generates, the third term is the road surface disturbance, and f_{dp} and f_{dr} of the forth term show the inertia force and the centrifugal force. Table 1 shows the parameter which are used for the numerical simulation (Hrovat, 1997), (Takahashi, 2003).

3. Controller design

Figure 2 shows the control system. The robustness of the system is guaranteed in the frequency domain in which it is assumed that the impact of road disturbance is small utilizing an H_∞ controller. Furthermore, it is possible to change the frequency weight according to the circumstance the vehicle is traveling under by designing gain scheduling control. In this chapter, the concrete control design method is shown.

3.1 Disturbance-accommodation control

It is known that typical irregularities on road surface are inversely proportional to the square of frequency in the low-frequency domain and they have the kind of power spectral density that is inversely proportional to four powers or more in the high-frequency domain. The effectiveness of designing control that can be merged with the feedforward control of the disturbance has been demonstrated (Nishimura et al., 1989). Techniques of control that accommodate disturbances in which power spectral density flattens in the limited frequency domain have been used to deal with various disturbances. The road disturbance model in this study has been assumed to be colored disturbances and input from four tires. The augmented system of the disturbance model and the controlled system model is as follows:

$$\begin{aligned} \dot{\mathbf{x}}_{wi}(t) &= \mathbf{A}_{wi}\mathbf{x}_{wi}(t) + \mathbf{B}_{wi}\mathbf{v}(t) \\ w_i(t) &= \mathbf{C}_{wi}\mathbf{x}_{wi}(t) \quad (i = 1, \cdots, 4) \end{aligned} \tag{5}$$

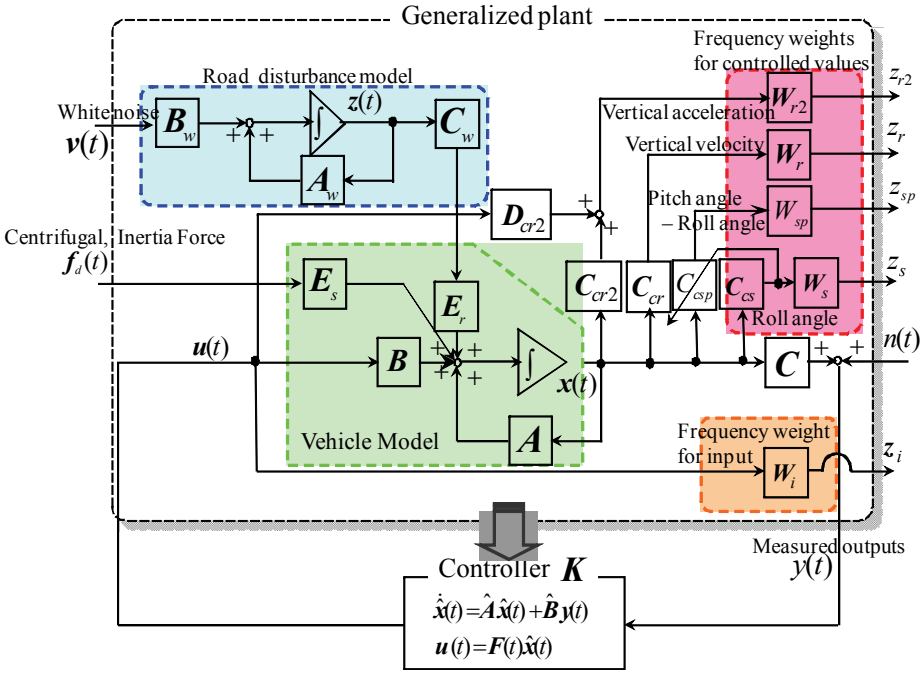

Fig. 2. Generalized plant

where $\mathbf{v}(t)$ is white noise. In this study, dynamics of the disturbance is represented as the low-pass characteristics.

$$\mathbf{A}_{wi}=\begin{bmatrix}-1 & 1 & 0\\ 0 & 0 & 1\\ 0 & -\omega_d^2 & -2\zeta_d\omega_d\end{bmatrix},\mathbf{B}_{wi}=\begin{bmatrix}0\\0\\ \omega_d^2\end{bmatrix}$$
$$\mathbf{C}_{wi}=\begin{bmatrix}1 & 0 & 0\end{bmatrix}\qquad (i=1,\cdots,4) \tag{6}$$

From Eqs. (4) and (5), the augmented system is derived.

$$\begin{bmatrix}\dot{\boldsymbol{x}}(t)\\ \dot{\boldsymbol{x}}_{wi}(t)\end{bmatrix}=\begin{bmatrix}\boldsymbol{A} & \boldsymbol{E}_r\boldsymbol{C}_{wi}\\ \boldsymbol{0} & \boldsymbol{A}_{wi}\end{bmatrix}\begin{bmatrix}\boldsymbol{x}(t)\\ \boldsymbol{x}_{wi}(t)\end{bmatrix}+\begin{bmatrix}\boldsymbol{B}\\ \boldsymbol{0}\end{bmatrix}\boldsymbol{X}^*(t)\boldsymbol{u}(t)+\begin{bmatrix}\boldsymbol{0}\\ \boldsymbol{B}_{wi}\end{bmatrix}\boldsymbol{v}(t)+\begin{bmatrix}\boldsymbol{E}_s\\ \boldsymbol{0}\end{bmatrix}\boldsymbol{f}_d(t)$$
$$\boldsymbol{y}(t)=\begin{bmatrix}\boldsymbol{C} & \boldsymbol{0}\end{bmatrix}\begin{bmatrix}\boldsymbol{x}(t)\\ \boldsymbol{x}_{wi}(t)\end{bmatrix} \tag{7}$$

The cutoff frequency of the low-pass filter is $\omega_d=50\times 2\pi\,\mathrm{rad/s}$ and the damping ratio is $\zeta_d=1/\sqrt{2}$. An optimal control input in the augmented system is

$$u^o(t)=-\mathbf{R}^{-1}\mathbf{B}^T\mathbf{P}_{11}\mathbf{x}(t)-\mathbf{R}^{-1}\mathbf{B}^T\mathbf{P}_{12}\mathbf{x}_{wi}(t) \tag{8}$$

$\mathbf{P}_{11}$ and $\mathbf{P}_{12}$ are unique positive definite solution of the following Riccati equation.

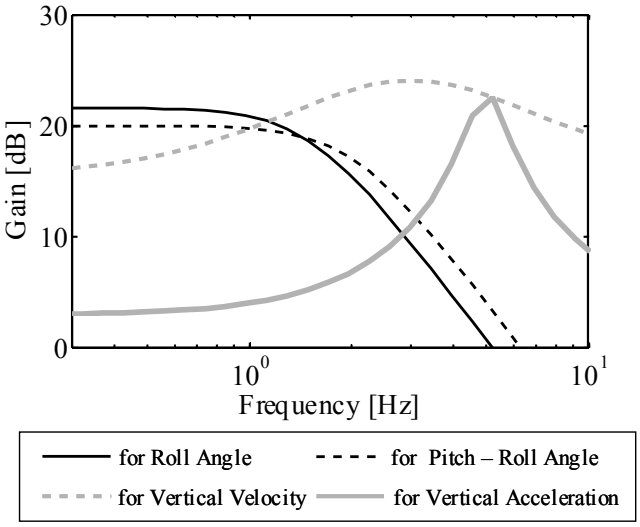

Fig. 3. Frequency Weights for Controlled Values

$$\mathbf{P}_{11}\mathbf{A} + \mathbf{A}^T\boldsymbol{P}_{11} - \mathbf{P}_{11}\mathbf{B}\mathbf{R}^{-1}\mathbf{B}^T\mathbf{P}_{11} + \mathbf{Q} = \mathbf{0} \tag{9}$$

$$\mathbf{P}_{11}\mathbf{E}_r\mathbf{C}_{wi} + \mathbf{P}_{12}\mathbf{A}_{wi} + \mathbf{A}^T\mathbf{P}_{12} - \mathbf{P}_{11}\mathbf{B}\mathbf{R}^{-1}\mathbf{B}^T\mathbf{P}_{12} = \mathbf{0} \tag{10}$$

From Eq.(8), it is confirmed that the feedback gain is decided unrelated to the quality of the disturbance and the feedforward gain is decided according to the quality of the disturbance.

3.2 Bilinear disturbance-accommodation H∞ control

It has been pointed out that the response level deteriorates in the frequency domain in which the estimated disturbance level is small when an unexpected disturbance is input (Nishimura et al., 1989). Improved robustness in the frequency domain is regarded as uncertainty in an augmented system (Kang et al., 1992).

In addition, to separate the control range in terms of the frequency domain, the frequency weighting in controlled variables is used. The frequency weightings $\boldsymbol{W}_r$ and $\boldsymbol{W}_{r2}$ are shown in Fig. 3. To improve ride comfort, these frequency weightings which have peaks near the body resonance frequency and near the frequency domain of 4 - 8 Hz, which make humans feel uncomfortable, are designed (Janeway, 1948).

Changes in body attitude should be decreased to improve steering stability. The controlled variable is the roll angle. The frequency weight $\boldsymbol{W}_s$ for the roll angle is designed in the low-frequency domain. Furthermore, the controlled variable is the relative angle of pitch and roll, and the pitch and roll angles caused by steering need to be synchronized to reduce the feeling of rolling. For both controlled variables, the frequency weight $\boldsymbol{W}_{sp}$ is designed in the low-frequency domain. In this study, H_∞ control theory (Umehara, 2005) and the disturbance accommodation control theory which are expanded to the bilinear system are applied to control of the semi-active suspension. To design of the generalized plant, the frequency weights for the controlled variable and control input are designed.

$$
\begin{aligned}
Q_c &\begin{cases} \dot{\mathbf{x}}_c(t) = \mathbf{A}_c\mathbf{x}_c(t) + \mathbf{B}_c\mathbf{x}_z(t) \\ \mathbf{z}_c(t) = \mathbf{C}_c\mathbf{x}_c(t) + \mathbf{D}_c\mathbf{x}_z(t) \end{cases} \\
Q_i &\begin{cases} \dot{\mathbf{x}}_i(t) = \mathbf{A}_i\mathbf{x}_i(t) + \mathbf{B}_i\mathbf{X}(t)^*\mathbf{u}(t) \\ \mathbf{z}_i(t) = \mathbf{C}_i\mathbf{x}_i(t) + \mathbf{D}_i\mathbf{X}(t)^*\mathbf{u}(t) \end{cases}
\end{aligned} \tag{11}
$$

where $\mathbf{x}_z$ represents the variable of the augmented system. $\mathbf{z}_c$ is the controlled variable and $\mathbf{z}_i$ is the output of the frequency weight for control input. The controlled model, the disturbance model, and the frequency weight are merged and the state-space representation of the generalized plant is as follows:

$$
\begin{aligned}
\dot{\mathbf{x}}_g(t) &= \mathbf{A}_g\mathbf{x}_g(t) + \mathbf{B}_1\boldsymbol{w}_g(t) + \mathbf{B}_2\mathbf{X}^*(t)\mathbf{u}(t) \\
\mathbf{z}(t) &= \mathbf{C}_1\mathbf{x}_g(t) + \mathbf{D}_{12}\mathbf{X}^*(t)\mathbf{u}(t) \\
\mathbf{y}(t) &= \mathbf{C}_2\mathbf{x}_g(t) + \mathbf{D}_{21}\mathbf{w}_g(t)
\end{aligned} \tag{12}
$$

where $\dot{\mathbf{x}}_g(t) = \begin{bmatrix} \mathbf{x} & \mathbf{x}_{wi} & \mathbf{x}_c & \mathbf{x}_i \end{bmatrix}^T$, $\mathbf{z}_g(t) = diag(\mathbf{z}_c, \mathbf{z}_i)$ and $\mathbf{w}_g(t) = \begin{bmatrix} \mathbf{v} & \mathbf{f}_d & \mathbf{w}_n \end{bmatrix}^T$. $\mathbf{w}_g$ represents the vector which includes road disturbances, the inertial forces, the centrifugal force vectors and measurement noise. The output vector y is the sprung mass velocity of each suspension. The H_∞ norm of transfer function G_{zw} from disturbance $\mathbf{w}_g$ of the generalized plant to evaluation output $\boldsymbol{z}$ is expressed making use of the L_2 gain of the time domain.

$$
\min_u \left\| \mathbf{G}_{zw} \right\|_\infty = \min_u \sup_w \frac{\left\| \mathbf{z} \right\|_2}{\left\| \mathbf{w}_g \right\|_2} =: \gamma^* \tag{13}
$$

where γ is the minimum H_∞ norm. The performance function is expressed by arbitrary γ.

$$
\begin{aligned}
&J(\boldsymbol{u}, \boldsymbol{w}_g) := \int_0^\infty [\boldsymbol{z}(t)\boldsymbol{z}(t) - \gamma^2 \boldsymbol{w}_g^T(t)\boldsymbol{w}_g(t)]dt \\
&= \int_0^\infty \left[\boldsymbol{x}_g(t)^T \boldsymbol{Q}\boldsymbol{x}_g(t) + 2\boldsymbol{x}_g(t)^T \boldsymbol{S}\boldsymbol{x}_g^*(t)\boldsymbol{X}(t)\boldsymbol{u}(t) + \boldsymbol{u}(t)^T \boldsymbol{X}^*(t)^T \boldsymbol{R}\boldsymbol{X}^*(t)\boldsymbol{u}(t) - \gamma^2 \boldsymbol{w}_g(t)^T \boldsymbol{w}_g(t) \right] dt
\end{aligned} \tag{14}
$$

The problem in Eq. (13) can be replaced with that in Eq. (14).

$$
J(\mathbf{u}^o, \mathbf{w}^o) := \min_u \max_w J(\mathbf{u}, \mathbf{w}_g) \tag{15}
$$

where $\mathbf{w}^o$ is the worst disturbance. $\mathbf{u}^o$ represents the optimal control input.

$$
\mathbf{u}^o(t) = -(\mathbf{D}_{12}^T\mathbf{D}_{12}\mathbf{X}^*(t))^{-1}(\mathbf{B}_2^T\mathbf{X}_u + \mathbf{S}^T)\mathbf{x}_g(t) \tag{16}
$$

The problem in Eq. (13) becomes that of calculating the saddle point solution, $J(\boldsymbol{u}^o, \boldsymbol{w}^o)$, which is acquired by actualizing optimal control input $\boldsymbol{u}^o$ under the worst disturbance, $\boldsymbol{w}^o$. Next, the following compensator is designed as an output feedback control problem.

$$
\hat{\dot{\mathbf{x}}}(t) = \hat{\mathbf{A}}\hat{\mathbf{x}}(t) + \hat{\mathbf{B}}\mathbf{y}(t) \tag{17}
$$

$$\hat{\mathbf{u}}(t) = \mathbf{F}(t)\hat{\mathbf{x}}(t) \tag{18}$$

The solution to this compensator is the center solution to a robust stabilization compensator for a bilinear system using solution **Y** of the Riccati algebraic equation. The details of each matrix are as follows:

$$\begin{aligned}
\hat{\mathbf{A}} &= \mathbf{A}_g + (\mathbf{B}_2 + \hat{\mathbf{B}}\mathbf{D}_{22})\mathbf{X}^*(t) + \gamma^{-2}\mathbf{B}_1\mathbf{B}_1^T\mathbf{X} - \hat{\mathbf{B}}(\mathbf{C}_2 + \gamma^{-2}\mathbf{D}_{21}\mathbf{B}_1^T\mathbf{X}) \\
\hat{\mathbf{B}} &= -(\boldsymbol{I} - \gamma^2\mathbf{Y}\mathbf{X})^{-1}(\mathbf{Y}\mathbf{C}_2^T + \mathbf{B}_1\mathbf{D}_{21}^T)(\mathbf{D}_{21}\mathbf{D}_{21}^T)^{-1} \\
\mathbf{F}(t) &= -(\mathbf{R}\mathbf{X}^*(t))^{-1}(\mathbf{B}_2^T\mathbf{X} + \mathbf{S}^T)
\end{aligned} \tag{19}$$

3.3 Gain schduling control

It has been reported that the feel of rolling reduces when the pitch angle always takes a positive value (Kawagoe et al., 1997). From the viewpoint of feeling by humans, we need to find a nonlinear relationship between roll and pitch angles (Sakai et al., 2006), (Yamamoto, 2006). The controller is scheduled in the time domain to achieve a positive pitch angle during slaloms. A gain scheduling controller that adapts the frequency weight, $a_p(t)$, of the frequency-shaped filter according to the variable parameter, $p(t)$, is introduced.

$$p(t) = a_p(t) \quad (p_{\min} \le p(t) \le p_{\max}) \tag{20}$$

The generalized plant which includes variable parameter, $p(t)$, is as follows:

$$\begin{aligned}
\dot{\mathbf{x}}_g(t) &= \mathbf{A}_g(p(t))\mathbf{x}_g(t) + \mathbf{B}_1\mathbf{w}_g(t) + \mathbf{B}_2\mathbf{X}^*(t)\mathbf{u}(t) \\
\mathbf{z}(t) &= \mathbf{C}_1(p(t))\mathbf{x}_g(t) + \mathbf{D}_{12}\mathbf{X}^*(t)\mathbf{u}(t) \\
\mathbf{y}(t) &= \mathbf{C}_2\mathbf{x}_g(t) + \mathbf{D}_{21}\mathbf{w}_g(t)
\end{aligned} \tag{21}$$

The parameter variable system which includes variable parameter, $p(t)$, in Eq. (21) is

$$\begin{bmatrix} \mathbf{A}_n(p(t)) & \mathbf{B}_n \\ \mathbf{C}_n & \mathbf{D}_n \end{bmatrix} = \sum_{i=1}^{2} \alpha_i \begin{bmatrix} \mathbf{A}_{ni} & \mathbf{B}_{ni} \\ \mathbf{C}_{ni} & \mathbf{D}_{ni} \end{bmatrix} \tag{22}$$

where

$$\begin{aligned}
\begin{bmatrix} \mathbf{A}_{n1} & \mathbf{B}_{n1} \\ \mathbf{C}_{n1} & \mathbf{D}_{n1} \end{bmatrix} &= \begin{bmatrix} \mathbf{A}_n(p_{\min}) & \mathbf{B}_n \\ \mathbf{C}_n(p_{\min}) & \mathbf{D}_n \end{bmatrix} \\
\begin{bmatrix} \mathbf{A}_{n2} & \mathbf{B}_{n2} \\ \mathbf{C}_{n2} & \mathbf{D}_{n2} \end{bmatrix} &= \begin{bmatrix} \mathbf{A}_n(p_{\max}) & \mathbf{B}_n \\ \mathbf{C}_n(p_{\max}) & \mathbf{D}_n \end{bmatrix}
\end{aligned} \tag{23}$$

At the top of the parameter box, $\mathbf{A}_{ni}$, $\mathbf{B}_{ni}$, $\mathbf{C}_{ni}$, $\mathbf{D}_{ni}$ are given

$$\begin{aligned}
a_1(p(t)) &= \frac{p_{\max} - p(t)}{p_{\max} - p_{\min}} \\
a_2(p(t)) &= \frac{p(t) - p_{\min}}{p_{\max} - p_{\min}}
\end{aligned} \tag{24}$$

$$\begin{aligned} \mathbf{F}_1(t) &= \mathbf{F}(t, p_{\min}) \\ \mathbf{F}_2(t) &= \mathbf{F}(t, p_{\max}) \end{aligned} \tag{25}$$

The gain scheduling controller, $\mathbf{F}(t,p)$, is as follows:

$$\mathbf{F}(t,p) = \sum_{i=1}^{2} \alpha_i(p)\mathbf{F}_i(t) \tag{26}$$

More concretely, the third power of the roll angle is used as variable parameter $p(t)$, to achieve nonlinearity and positive value conversion of the pitch.

$$p(t) = 1000\phi_r^3(t) + 2.2 \tag{27}$$

To achieve a nonlinear relationship between the roll and pitch angles, relative angle of the roll to the pitch is scheduled by using the matrix C_{csp} shown in Fig. 2.

$$\begin{aligned} \mathbf{C}_{sp\min} &= \begin{bmatrix} 0 & -40 & -1 & 0 & 0 & 0 & \cdots \end{bmatrix} \\ \mathbf{C}_{sp\max} &= \begin{bmatrix} 0 & 40 & -1 & 0 & 0 & 0 & \cdots \end{bmatrix} \end{aligned} \tag{28}$$

The control input is calculated based on bilinear disturbance-accommodation H_∞ control and gain schduling control.

4. Simulation result

In order to verify the effectiveness of the proposed method, the numerical simulations were carried out. Figure 4 has the results of numerical simulation for the slalom. The road width in the simulation was about 3 m, and the velocity of the vehicle was 15 m/s (=54 km/h) and a road disturbance of ISO standard C level was used.

The time history of the scheduling parameter in case 1 is shown in Fig. 5. It was confirmed that the scheduling parameter is changed according to the roll angle caused by steering. The time histories of the body roll and pitch angles are shown in Figs. 6 and 7 respectively. From the results, it was confirmed that the roll angle is reduced by comparison with passive control.

Figure 8 shows the relationship between the roll and pitch angles. The results confirmed that the proposed method achieves the nonlinear relationship between the pitch and roll angles.

Figure 9 shows the PSD of vertical acceleration. The result confirmed that the vertical acceleration near the body resonance frequency and in the frequency domain of 4 - 8 Hz, which make humans feel uncomfortable, can be reduced. In addition, ride comfort that takes into consideration human sensitivity to vibrations in the slalom can be improved.

Figure 10 shows the maximum reduction ratio of RMS. The results confirmed that the proposed method can reduce the body vertical acceleration as well as skyhook control and the soft fixed model. In addition, the body roll angle, which cannot be decreased with these controls, can be reduced as well as the hard fixed model.

Figure 11 shows the simulation course in case 2. The simulation results in case 2 are shown in Figs. 12 to 17. All results verified control could be accomplished that was equal to case 1. The results in Fig.16 especially confirmed that the body attitude, which changes more drastically in the slalom, can be reduced. In addition, the nonlinear relationship between the pitch and roll angles can be achieved.

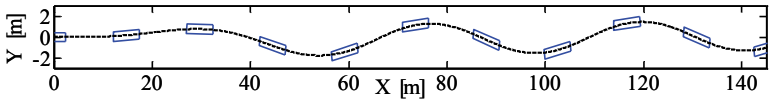

Fig. 4. Simulation Course (Case 1)

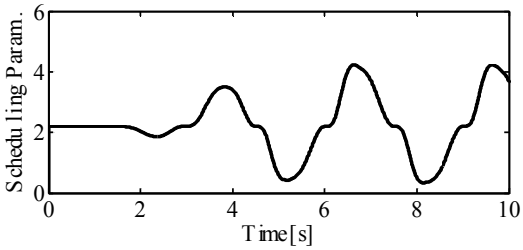

Fig. 5. Scheduling Parameter (Case 1)

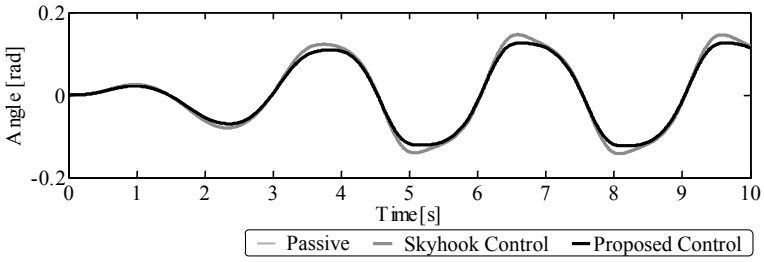

Fig. 6. Roll Angle (Case 1)

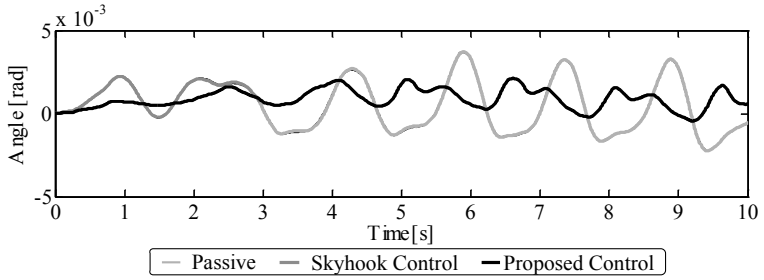

Fig. 7. Pitch Angle (Case 1)

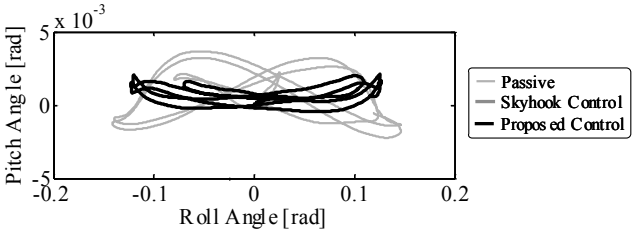

Fig. 8. Relationship between Roll Angle and Pitch Angles (Case 1)

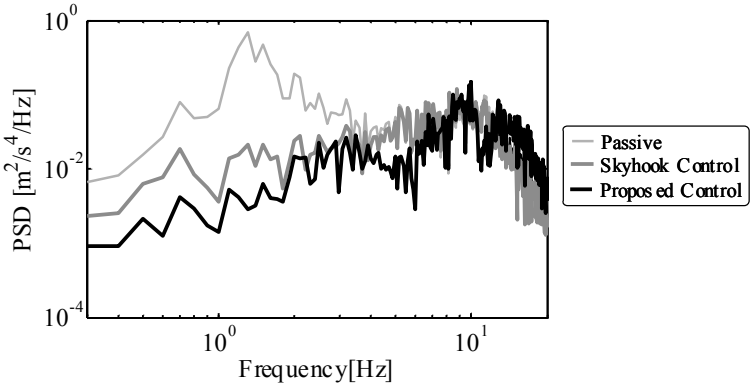

Fig. 9. PSD of Vertical Acceleration (Case 1)

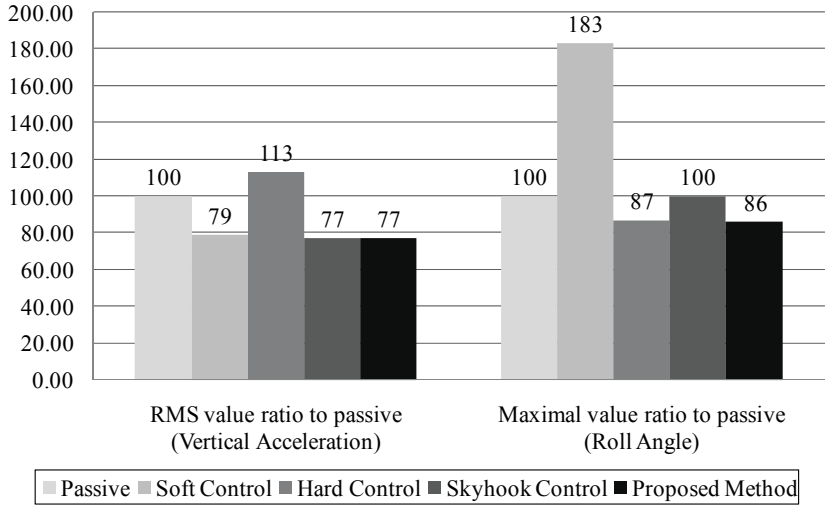

Fig. 10. RMS Values and Peak Values for Each Method (Case 1)

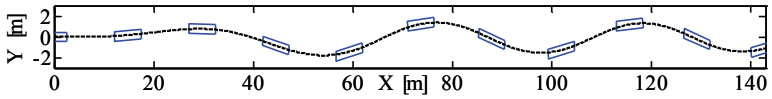

Fig. 11. Simulation Course (Case 2)

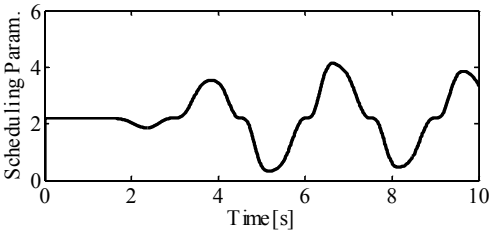

Fig. 12. Scheduling Parameter (Case 2)

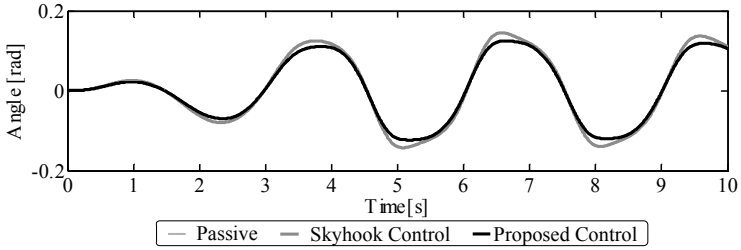

Fig. 13. Roll Angle (Case 2)

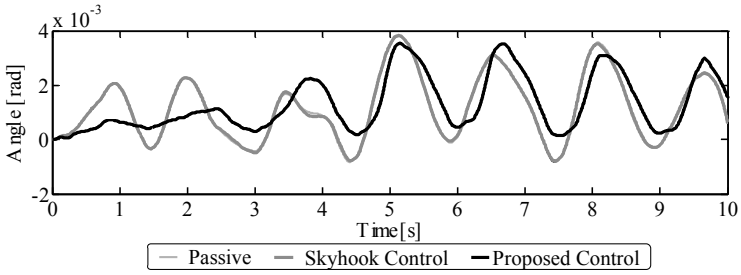

Fig. 14. Pitch Angle (Case 2)

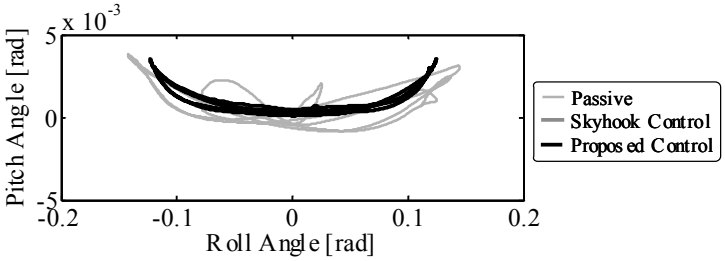

Fig. 15. Relationship between Roll Angle and Pitch Angles (Case 2)

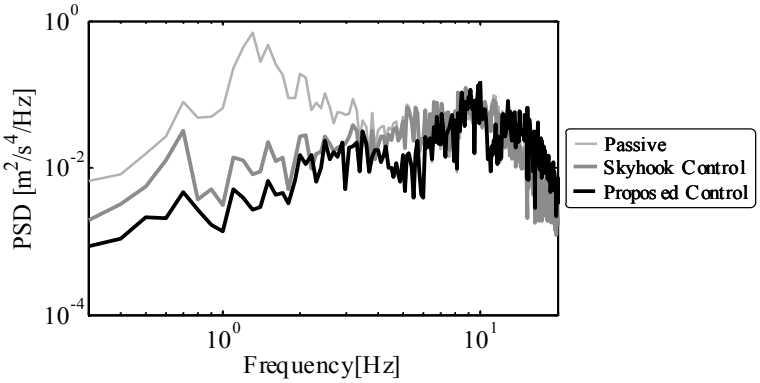

Fig. 16. PSD of Vertical Acceleration (Case 2)

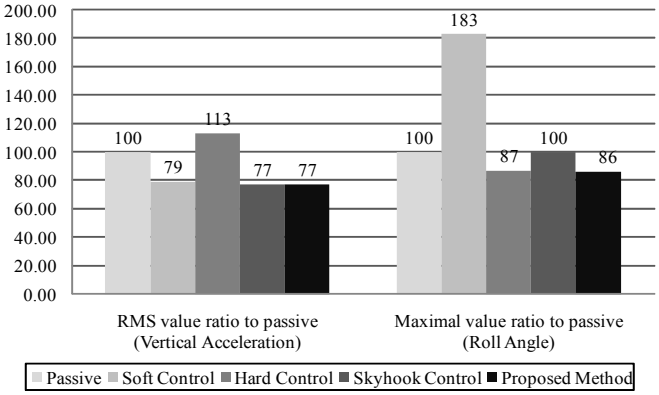

Fig. 17. RMS Values and Peak Values for Each Method (Case 2)

5. Conclusion

Controller design to achieve variable stiffness and a variable damping semi-active suspension system was attained by applying disturbance accommodation control theory, bilinear H^{∞} control theory, and gain scheduling control theory to improve the efficiency of ride comfort and vehicle behavior during steering. Several numerical simulations confirmed that ride comfort in the frequency domain, in which humans feel uncomfortable, can be improved without deteriorating passenger ride comfort in comparison with skyhook control. The change in body attitude when steering can also be reduced and vehicle behavior with synchronized phase difference between roll and pitch can be acquired. The results confirmed that both ride comfort and steering stability can be improved in a balanced manner.

6. References

Ohsaku, S., Sampei, M., Shimizu, E. and Tomida, K. (2000), Nonlinear Control for Semi-Active Controlled Suspension, *Journal of the Society of Instrument and Control Engineers*, Vol.39, No.2, pp.126-129.

Hrovat, D. (1993), Application of optimal control to advanced automotive suspension design, Transaction on ASME: Journal of Dynamic Systems, Measurement, and Control, pp.328-342.

Hrovat, D. (1997), Survey of advanced suspension developments and related optimal control applications, *Automatica*, Vol.33, No.10, pp.1781-1816.

Abdel-Hardy, M.B.A. and Crolla, D.A. (1989), Theoretical analysis of active suspension performance using a four-wheel model, *Proceedings of the Institution of Mechanical Engineers*, No.203(D), pp.125-135.

Abdel-Hardy, M.B.A. and Crolla, D.A. (1992), Active suspension control algorithms for a fourwheel vehicle model, *International Journal of Vehicle Design*, Vol.13, No.2, pp.144-158.

Hanamura, Y., Fujita, K., Araki, Y., Oya, M., and Harada, H. (1999), Control of Vehicle Maneuverability and Stability of 4 Wheeled Vehicle by Active Suspension Control with Additional Vertical Load Control, *Transactions of the Japan Society of Mechanical Engineers, Series C*, Vol.65, No.629, pp.236-243.

Doi, S., Yamaguchi, H., Iwama, N, Hayashi, Y. (1992), Study of Semiactive Control by Optimum Damping Adjustment (Suspension Control Using Frequency-Shaped Functionals), *Transactions of the Japan Society of Mechanical Engineers, Series C*, Vol.58, No.549, pp.3297-3304.

Yoshida, K., Kumamaru, T. and Nagata, S. (2006), Frequency-Shaped Gain-Scheduling Control for Automotive Semi-Active Suspension, *Proceedings of The 8th International Conference on Motion and Vibration Control*.

Janeway, R.N. (1948), *SAE Journal*, pp.48.

Sakai, H., Ono, E., Yamamoto, Y., Fukui, K., Oki, M. and Yasuda, E. (2006), Improvement of Roll Feeling Based on Visual Sensitivity, *Toyota Technical Review*, Vol.55, No.1, pp.20-25.

Yamamoto, M. (2006), History and Future of Vehicle Dynamics, *Toyota Technical Review*，Vol.55, No.1, pp.6-13.

Kawagoe, K. (1997), A Study of Vehicle Roll Behavior, *Journal of Society of Automotive Engineers of Japan*, Vol.51, No.11, pp.20-24.

Bakker, E., Nyborg, L., and Pacejka, H. B. (1987), Tyre Modelling for Use in Vehicle Dynamics Studies, *SAE paper*, 870421.

Bakker, E., Pacejka, H. B. and Nyborg, L. (1989), A New Tire Model with an Application in Vehicle Dynamics Studies, *SAE paper*, 890087.

Takahashi, T. (2003), Modeling, Analysis and Control Methods for Improving Vehicle Dynamic Behavior (Overview), *R&D Review of Toyota CRDL*, Vol.38, No.4, pp.1-9.

Nishimura, H., Yoshida, K. and Shimogo, T. (1989), Optimal Active Dynamic Vibration Absorber for Multi-Degree-of-Freedom Systems: Feedback and Feedforward Control Using a Kalman Filter, *Transactions of the Japan Society of Mechanical Engineers, Series C*, Vol.55，No.517, pp.2321-2329.

Kang, S., and Yoshida, K. (1992), Vibration Isolation Control with Feedforward Link using H_∞ Control Theory, *Transactions of the Japan Society of Mechanical Engineers, Series C*, Vol.58, No.556, pp.3627-3633.

Umehara, R., Otsuki, M., and Yoshida, K., (2005) Bilinear Robust Control Method and Its Application to Semi-Active Suspension for Railway Vehicle, *Transactions of the Japan Society of Mechanical Engineers, Series C*, Vol.71, No.701, pp129-136.

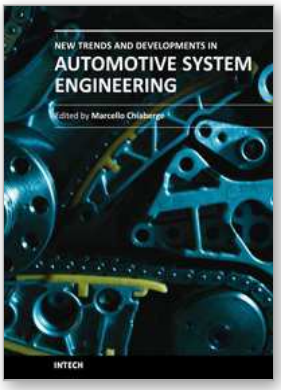

New Trends and Developments in Automotive System Engineering
Edited by Prof. Marcello Chiaberge

ISBN 978-953-307-517-4
Hard cover, 664 pages
Publisher InTech
Published online 08, January, 2011
Published in print edition January, 2011

In the last few years the automobile design process is required to become more responsible and responsibly related to environmental needs. Basing the automotive design not only on the appearance, the visual appearance of the vehicle needs to be thought together and deeply integrated with the â€œpowerâ€ developed by the engine. The purpose of this book is to try to present the new technologies development scenario, and not to give any indication about the direction that should be given to the research in this complex and multi-disciplinary challenging field.

InTech Europe
University Campus STeP Ri
Slavka Krautzeka 83/A
51000 Rijeka, Croatia
Phone: +385 (51) 770 447
Fax: +385 (51) 686 166
www.intechopen.com

InTech China
Unit 405, Office Block, Hotel Equatorial Shanghai
No.65, Yan An Road (West), Shanghai, 200040, China
中国上海市延安西路65号上海国际贵都大饭店办公楼405单元
Phone: +86-21-62489820
Fax: +86-21-62489821